*Biochemical Journal* (2020) **477** 1227–1240
https://doi.org/10.1042/BCJ20190536

Research Article

# Amyloid β chaperone — lipocalin-type prostaglandin D synthase acts as a peroxidase in the presence of heme

Margaret Phillips[1], Bhuvaneswari Kannaian[1], Justin Ng Tze Yang[1], Ralf Kather[2], Mu Yuguang[1], Jeffrey R. Harmer[2] and Konstantin Pervushin[1]

[1]School of Biological Sciences, Nanyang Technological University, Singapore; [2]Centre for Advanced Imaging, The University of Queensland, St Lucia, QLD 4072, Australia

**Correspondence:** Konstantin Pervushin (KPervushin@ntu.edu.sg)

The extracellular transporter, lipocalin-type prostaglandin D synthase (L-PGDS) binds to heme and heme metabolites with high affinity. It has been reported that L-PGDS protects neuronal cells against apoptosis induced by exposure to hydrogen peroxide. Our study demonstrates that when human WT L-PGDS is in complex with heme, it exhibits a strong peroxidase activity thus behaving as a pseudo-peroxidase. Electron paramagnetic resonance studies confirm that heme in the L-PGDS–heme complex is hexacoordinated with high-spin Fe(III). NMR titration of heme in L-PGDS points to hydrophobic interaction between heme and several residues within the β-barrel cavity of L-PGDS. In addition to the transporter function, L-PGDS is a key amyloid β chaperone in human cerebrospinal fluid. The presence of high levels of bilirubin and its derivatives, implicated in Alzheimer's disease, by binding to L-PGDS may reduce its chaperone activity. Nevertheless, our ThT binding assay establishes that heme and heme metabolites do not significantly alter the neuroprotective chaperone function of L-PGDS. Guided by NMR data we reconstructed the heme L-PGDS complex using extensive molecular dynamics simulations providing a platform for mechanistic interpretation of the catalytic and transporting functions and their modulation by secondary ligands like Aβ peptides and heme metabolites.

## Introduction

Lipocalin-type prostaglandin D synthase (L-PGDS) is a multifunctional protein known to bind to several lipophilic molecules with the low dissociation constant, through hydrophilic and hydrophobic interactions [1–3]. These small ligands bind inside the hydrophobic cavity of L-PGDS, which is larger than any other lipocalin, and thus undergoes a global conformational change resulting in a more compact 3D complex structure [4,5]. L-PGDS is involved in the up-regulation of several neurological processes and its expression levels play a critical role in numerous pathological conditions [6,7]. L-PGDS is also the second most abundant protein in human cerebrospinal fluid (CSF) after albumin [8] and has been shown to play an important role in the inhibition of Aβ aggregation by binding to monomeric Aβ as well as breaking down the pre-formed Aβ fibrils. It has been observed that the expression of *ptgds* gene is up-regulated in Alzheimer's disease (AD) and is associated with the presence of amyloid plaques [9,10]. The expression of L-PGDS in the prefrontal cortex of the brain is also associated with the clinical and pathological traits of AD [10,11].

Aggregation of the amyloid β peptide (amyloidosis) has been implicated in AD progression. Conformational alterations in Aβ peptide lead to its conversion from a soluble peptide to an insoluble aggregate which is considered as a key mechanism in the pathogenesis of neurodegenerative diseases such as AD [12,13]. Upon direct interaction with Aβ, iron (III) and copper (II) are reduced producing partially reduced oxygen species (PROS) [14–16]. These reactive oxidative species are involved in

Received: 24 July 2019
Revised: 7 February 2020
Accepted: 12 February 2020

Accepted Manuscript online: 13 February 2020
Version of Record published: 9 April 2020

Biochemical Journal (2020) 477 1227–1240
https://doi.org/10.1042/BCJ20190536

neuronal death linked to AD [17]. Although Fe has not been directly associated with amyloidosis, it has been shown to greatly influence oxidative stress, a pathological feature in AD [18,19]. Heme (ferriprotoporphyrin IX) is a Fe containing prosthetic group that binds to Aβ with high affinity thereby preventing Aβ aggregation and also resulting in heme deficiency in AD patients [20]. Since Aβ binds to both heme-a and heme-b, it induces an AD dependent change in heme regulation [20]. Previous reports have suggested that heme-b concentration increases by 250% while heme-a concentration decreases by 26% in an AD patient brain when compared with a healthy control brain [20]. To compensate for the low bioavailability of heme-a, the levels of heme-b increase in AD patient brain [20]. An increase in heme concentration has been linked to oxidative stress and mitochondrial decay [21]. Elevation in heme degradation products such as bilirubin is also observed in AD as a direct result of heme regulation [22]. The antibody 6E10 which recognizes the N-terminus of Aβ peptide and is capable of breaking down pre-formed fibrils failed to displace heme from the Aβ–heme complex or inhibit its peroxidase activity signifying high affinity of heme for Aβ [23]. The Aβ–heme complex also behaves as a peroxidase and since peroxidases oxidize several organic substrates with little selectivity, the peroxidase activity of the Aβ–heme complex could be responsible for the oxidative damage observed in AD brain [23].

Reactive oxygen intermediates (ROI) such as superoxide anion ($O_2^-$) and hydrogen peroxide ($H_2O_2$) are produced in all mammalian cells and are produced either during cellular metabolism or through the activation of certain enzymes responding to exogenous stimuli [24–27]. ROS being toxic to cells is tightly regulated by several mechanisms particularly involving the ROS scavenging enzymes such as catalase, superoxide dismutase and glutathione peroxidase [24–29]. A slight increase in the intracellular ROS concentration might act as a mytogenic stimulus thereby increasing cellular proliferation [30,31] and having an inhibitory effect on cellular apoptosis [28,32, 33]. In fact, it is higher concentrations of $H_2O_2$ in the cell that promotes neuronal apoptosis and causes a drop in the cytosolic pH further promoting apoptotic signaling [33–37]. It can, therefore, be rationalized that any mechanism that reduces the hydrogen peroxide concentration within the cell, such that the resulting oxidation is directed towards a controlled set of small ligands rather than the promiscuous oxidation of cellular lipids and nucleotides may perhaps lower the cell death and may have a neuroprotective effect. Catalase, an intracellular, tetrameric heme binding enzyme is capable of converting $H_2O_2$ to molecular oxygen and water when hydrogen peroxide concentrations are high [38,39]. At low $H_2O_2$ concentration, and in the presence of 'electron donors' (alcohols, nitrites and formats) catalases can acts as peroxidases [40]. Unlike catalases, the glutathione peroxidases (GPx) is the main enzyme in the cell responsible for the reduction in hydrogen peroxide to water using a variety of electron-donating molecules [40,41] in the process getting oxidized to its disulfide form (GSSG). The oxidized form is converted back to the reduced GSH by glutathione reductase utilizing NADPH as a reductant [40]. Thus both catalases and glutathione peroxidases are main scavengers of hydrogen peroxide in the cell tightly controlling the resulting free radicals.

Recently, Fukuhara et al. [42] reported for the first time, the protective role of L-PGDS in $H_2O_2$ induced apoptosis. L-PGDS was identified as a scavenger of ROS *in vitro* due to its ability to bind the free radicals produced by the breakdown of $H_2O_2$. This involved the oxidation of the thiol group of its Cys 65 residue. Moreover, the oxidized L-PGDS did not lose its ability to bind small lipophilic ligands such as retinoic acid and biliverdin thus emphasizing its multifunctional and possibly neuroprotective role in several neurodegenerative diseases [42].

Heme binding affinities of C65A/C167A and W112F/C167A substituted human L-PGDS have been characterized by ITC and induced circular dichroism studies [1,2]. Here, we demonstrate for the first time that WT L-PGDS can extract heme from Aβ–heme complex thus generating an efficient peroxidase system where unlike Aβ–heme complex the resulting oxidation is channeled to small lipophilic ligands transported by L-PGDS. We characterize the resulting heme L-PGDS complexes using tryptophan quenching, UV/Vis spectroscopy, cw EPR and solution-state NMR spectroscopy.

# Methods

## Protein expression and purification

The pNIC-CH2 vector carrying the L-PGDS gene with a C-terminal hexahistidine tag was transformed into Rosetta 2 DE3 Singles *Escherichia coli* cells (Novagen). The first 22 amino acids encoding the signal peptide was removed from the L-PGDS gene. The transformed cells were incubated at 37°C until the $OD_{600}$ reaches 0.8–1.0. Then, 1 mM IPTG was added to overexpress the protein and the cells were kept incubated at 37°C for 4 h before harvesting. To produce the $^{15}N$ labeled L-PGDS, the cells were grown at 37°C in the M9 media

containing 1 g/l $^{15}N$ $NH_4Cl$, until the $OD_{600}$ reaches 0.6. The cells were then induced with 0.5 mM IPTG and kept incubated at 18°C overnight. Expression and purification of WT-L-PGDS was done following the procedure from Kannaian et al. [43]. Liu et al. had reported wild-type (WT) human L-PGDS expressed and purified in *E. coli* was active but was consistently bound to fatty acids [44]. To reduce the lipid contamination, bound to human WT-L-PGDS, we used the refolded protein in all the assays. In brief, the protein was first purified using Ni-affinity chromatography and then unfolded by the addition of 8 M urea. The unfolded protein was then refolded by dialysis at 4°C and then passed through Superdex 75 10/300 GL column.

## Preparation of monomeric Aβ

Aβ(1–40), Aβ(25–35) and Aβ(1–16) peptides were purchased from China peptides (Suzhou, China). 1,1,1,3,3,3-hexafluoro-2-propanol (HFIP) treated Aβ(1–40) and Aβ(25–35) peptides were incubated at room temperature for 1 h and then lyophilized to remove the solvent. The peptide film was initially dissolved in a small volume of 100 mM NaOH and then diluted with the desired buffer. Peptide Aβ(1–16) was water soluble and was directly dissolved in required buffer.

## UV/Vis absorption spectroscopy

The UV/Vis absorption spectra were measured on Cytation 5 cell imaging multimode reader (BioTek Instruments) at 25°C in a 96-well plate (Costar®) for the wavelength range of 350–650 nm. Heme binding to 5 μM L-PGDS in 50 mM sodium phosphate buffer at pH 7.5 was monitored by the addition of increasing concentrations of heme from a 2.5 mM stock solution of heme in 0.1% NaOH (as described previously [45,46]). For Aβ (1–40) and Aβ (1–16) complex with heme the amyloid β peptides were freshly prepared as mentioned above and heme from fresh heme stock was added to get a final molar ratio of 1 : 1 (5 μM peptide with 5 μM heme) in sodium phosphate buffer at pH 7.5. After incubation of the amyloid β/heme complex for 1 h, 5 μM refolded WT L-PGDS was added in a 1 : 1 molar ratio to the complex and the UV/Vis spectra was recorded after gentle mixing. Heme alone was used as a blank and the differential spectra of all heme-containing samples were obtained after free heme subtraction.

## Tryptophan fluorescence quenching assay

A fresh 2.5 mM heme stock was prepared in 0.1% NaOH. From this stock, increasing concentration of heme was added to WT L-PGDS in 50 mM sodium phosphate (pH 7.5) buffer with the final concentration of the protein adjusted to 5 μM. A 100 μl of L-PGDS/heme complex was added to the Corning Costar® 96-well black, opaque, flat bottom plate after a 30 min incubation at room temperature. The intrinsic tryptophan fluorescence of L-PGDS was then measured using Cytation 5 cell imaging multimode (Biotek Instrument Inc., U.S.A.) reader with $\lambda_{ex} = 295$ nm and $\lambda_{em} = 340$ nm. As described previously, the Mass law equation for single binding was used to calculate the apparent dissociation constant ($K_d$) value for heme binding to L-PGDS with the following fitting equation [2]:

$$F = \left( \left( \frac{\left( (2^*[P_o]) - [L_o] - K_d + \left( (([L_o] + K_d - (n^*[P_o]))^2 + (4^*K_d^*n^*[P_o]) \right)^{\frac{1}{2}} \right) \right)^*(F_o - F_{min})}{2^*n^*[P_o]} \right) + F_{min} \right) \quad (1)$$

## Electron paramagnetic resonance spectroscopy

Two hundred micromolar WT L-PGDS in 20 mM HEPES, 100 mM NaCl, pH 7.5 with 200 μM heme (1 : 1) complex was used to record the X-band (9.3835 GHz) CW EPR spectra with a Bruker Biospin Elexsys E500 EPR spectrometer fitted with a Bruker superhigh Q cavity and a flow-through Oxford cryostat (CF935LT) in conjunction with an Oxford Instruments ITC503 variable-temperature controller. Measurements were made at 7.5 K using a modulation frequency of 100 kHz, modulation amplitude of 0.5 mT and a microwave power of 5 mW. The magnetic field was calibrated with a Bruker ER 036TM Teslameter.

Biochemical Journal (2020) 477 1227–1240
https://doi.org/10.1042/BCJ20190536

## NMR titration

NMR spectroscopy experiments were carried out in Bruker Avance 700 MHz with triple resonance *z*-axis gradient cryoprobe and Bruker DRX 600-MHz spectrometer equipped with a cryoprobe at 298 K. Uniformly $^{15}N$ labeled L-PGDS sample was prepared in 50 mM sodium phosphate buffer, pH 7.5 at a concentration of 0.25 mM with 5% $D_2O$ and 50 µM DSS (4,4-dimethyl-4-silapentane-1-sulfonic acid, used as NMR standard for calibration). To identify the key residues of L-PGDS involved in heme binding, two dimensional $^{1}H$–$^{15}N$ HSQC spectrum of $^{15}N$ labeled WT refolded L-PGDS was recorded at 25°C as a reference. Freshly prepared heme from a 2.5 mM stock solution was prepared in 0.1% NaOH and was gradually added into the L-PGDS sample before acquiring the 2D $^{1}H$–$^{15}N$ HSQC spectrum at each titration step. Spectra were referenced with respect to DSS and then overlapped to check if the cross-peaks showed any shift or change in signal intensity. Data were processed in Topspin 3.5 (Bruker Corporation) and then analyzed using computer-aided resonance assignment (CARA) (www.nmr.ch) [47].

## Model construction of L-PGDS–heme complex

Heme docking to L-PGDS was performed using the High Ambiguity-Driven biomolecular DOCKing (HADDOCK) webserver easy interface mode [48]. The co-ordinates of heme ligand were extracted from the protein data bank [49] and the structure of L-PGDS protein in its Apo form (PDB ID: 4IMN) [50] were selected as the two molecules for docking input. The residues as identified to be involved in LPGDS–heme interaction through chemical shift perturbation using NMR titration were selected as active residues. The option to define passive residues automatically around the active residues was enabled. The best structure of the top-scoring cluster is selected as the binding pose for classical molecular dynamics (MD) simulations.

## Model construction of L-PGDS–bilirubin–Aβ(1–40) complex

Bilirubin docking to L-PGDS was performed using the HADDOCK web server easy interface mode [48]. The co-ordinates of bilirubin ligand were extracted from the protein data bank [49] and the structure of L-PGDS protein in its Apo form (PDB ID: 4IMN) [50] were selected as the two molecules for docking input. The residues as identified to be involved in LPGDS–bilirubin interaction through chemical shift perturbation using NMR titration were selected as active residues. The option to define passive residues automatically around the active residues was enabled. The best structure of the top-scoring cluster is selected as the initial structure to construct the model of L-PGDS–bilirubin–Aβ(1–40) complex. This model was superimposed onto our recent model of the L-PGDS–Aβ(1–40) complex [43], and the co-ordinates of L-PGDS, bilirubin and Aβ(1–40) was extracted to generate the model of L-PGDS–bilirubin–Aβ(1–40) complex.

## Energy minimization and molecular dynamics simulations

The constructed models of L-PGDS–heme and L-PGDS–bilirubin–Aβ(1–40) complexes were further subjected to energy minimization and explicit solvent classical MD simulations using the Gromacs [51] 5.1.2 package. The CHARMM36m [52] force field was used for amino acid residues of L-PGDS and Aβ(1–40), whereby the parameter sets have been recently optimized for simulations of Intrinsically Disordered and folded proteins. Charmm [52] force field parameters for heme were used and parameters for bilirubin were obtained from the CHARMM-GUI webserver [53]. Both systems were solvated with CHARMM-modified TIP3P [54] water in a cubic box with a distance of 1.2 nm from the solute to the box edge. $Na^+$ and $Cl^-$ counterions were added to neutralize the system and to achieve a salt concentration of 0.15 M. Bonds containing hydrogen atoms were constrained using the LINCS [55] algorithm, to enable a time step of 2 fs. Particle Mesh Ewald [56] was used with a cutoff of 1.2 nm for electrostatics, and a cutoff of 1.2 nm was used for van der Waal's interactions. Steepest Descent energy minimization was performed until a force convergence of 1000.0 kJ/mol/nm is reached to remove any initial bad contacts. An equilibration of 1 ns in the NVT ensemble was performed prior to the start of production simulation. The temperature of the system was maintained at 300 K using the V-rescale [57] thermostat. Three repeats of classical MD simulations of 100 ns were performed for each system with different random initial velocities. Trajectory frames were saved every 2 ps.

To evaluate the quality of our simulation model, we generated a Ramachandran plot for L-PGDS residues of the representative model in the L-PGDS–heme complex using the Wincoot software. We also calculated the root mean square deviation (RMSD) of the L-PGDS–heme complex as a function of simulation time over three simulation repeats.

## Obtaining simulation representative models for each system

Following the completion of MD simulations, the last 50 ns of each simulation repeat were combined for the respective systems. Geometric clustering was performed using the Gromos algorithm of the in-built Gromacs [51] gmx cluster tool with the ligand as the clustering group and a cutoff of 0.25 nm to obtain simulation representative models of L-PGDS–heme and L-PGDS–bilirubin–Aβ(1–40) complexes.

## Thioflavin T assay

Inhibition of Aβ aggregation by L-PGDS was studied by Thioflavin T (ThT) assay. ThT is a small fluorescent dye that emits enhanced fluorescence by binding to the β-sheet structure of the amyloid fibrils. To study the inhibitory effect of LPGDS and LPGDS–BR complex, monomeric Aβ40 and Aβ(25–35) peptides were incubated with and without L-PGDS and L-PGDS/BR complex at a 10 : 1 ratio of Peptide: Protein in 20 μM ThT, 20 mM HEPES, 100 mM NaCl, 2 mM TCEP (pH-7.5). Experiments were carried out in triplicates in NUNC 96 well black plate with incubation at 37°C in TECAN infinite M200 Pro microplate reader with orbital shaking before each measurement. The plate was sealed completely to prevent evaporation and measurements were read with an excitation wavelength at 440 nm and emission at 485 nm.

## Peroxidase assay

The peroxidase activity of WT refolded L-PGDS/heme complex and the Aβ(1–40)/heme complex was monitored by measuring the oxidation of the substrate-3,3′,5,5′-tetramethylbenzidine (TMB) by hydrogen peroxide ($H_2O_2$) using the TMB/E single reagent (blue color, Horseradish Peroxidase substrate kit from MERCK containing liquid solution TMB −1.25 mM/l and hydrogen peroxide −2.21 mMol/l) at 652 nm absorbance via Cytation 5 cell imaging multimode reader (BioTek Instruments). The peroxidase activity of both L-PGDS/heme and of Aβ(1–40)/heme was tested for 5 μM complex for 30–60 min, in triplicates, at 25°C in a 96-well plate (Costar®). Orbital shaking for 10 s before each absorbance reading insured thorough mixing of substrates with heme complexes.

## Isothermal titration calorimetry (ITC)

The calorimetric experiment was performed with Microcal ITC200 (Malvern, U.S.A.), in 50 mM sodium phosphate buffer (pH 7.5) at 25°C. WT refolded L-PGDS (200 μM) in the injection syringe was reversely titrated into 2 μM TMB substrate (purchased from Sigma–Aldrich) in the cell. Titration experiment consisted of 19 injections spaced at 360 s intervals. The injection volume was 2 μl and the cell was continuously stirred at 750 rpm. The observed enthalpy changes ($\Delta H°$) for binding were directly calculated and evaluated from integrated heats using a sequential binding site model available in MicroCal Origin 7.0 software.

# Results

UV/Visible absorption spectroscopy was used to confirm the heme binding to refolded, human WT L-PGDS. The Soret band for free heme appears as a broad peak ∼386–390 nm. The absorption spectrum of heme bound to L-PGDS shows a red shift of the Soret band to 404 nm (∼15 nm) (Figure 1A). The shape, intensity and position of this Soret band are distinct from that of free heme indicating that heme is in a complex with L-PGDS [58–60]. The reducing agent sodium dithionite causes a further shift of the Soret band to 420 nm with an increased intensity of the single α, β band at 560 nm showing the reduction in the heme–L-PGDS complex to its ferrous form with hexa-co-ordinated Fe(III) heme [58–60]. The characteristic spectral changes observed when heme was added in increasing concentration to L-PGDS and the Soret band shift of free heme to bound state heme was monitored (Supplementary Figure S1).

The intrinsic tryptophan fluorescence quenching assay also confirmed heme binding to WT L-PGDS. We observed complete quenching of tryptophan fluorescence intensity at a 1 : 1 molar ratio of L-PGDS to heme (Supplementary Figure S2). The apparent dissociation constant $K_d$ for heme binding to WT L-PGDS ($K_d = 40$ nM ± 0.9) was then calculated by fitting the relative fluorescence intensity of L-PGDS versus the molar ratio of heme to WT L-PGDS concentration to a single binding site model ($n = 1$) as reported previously by Kume et al. [2]. Both UV/Vis and tryptophan quenching measurements have thus demonstrated high-affinity binding for heme, which is in good agreement with previously published high-affinity binding for C65A/C167A and W112F/C167A substituted human L-PGDS–heme complexes ($K_d = 20$ nM ± 0.8) [1,2].

*Biochemical Journal* (2020) **477** 1227–1240
https://doi.org/10.1042/BCJ20190536

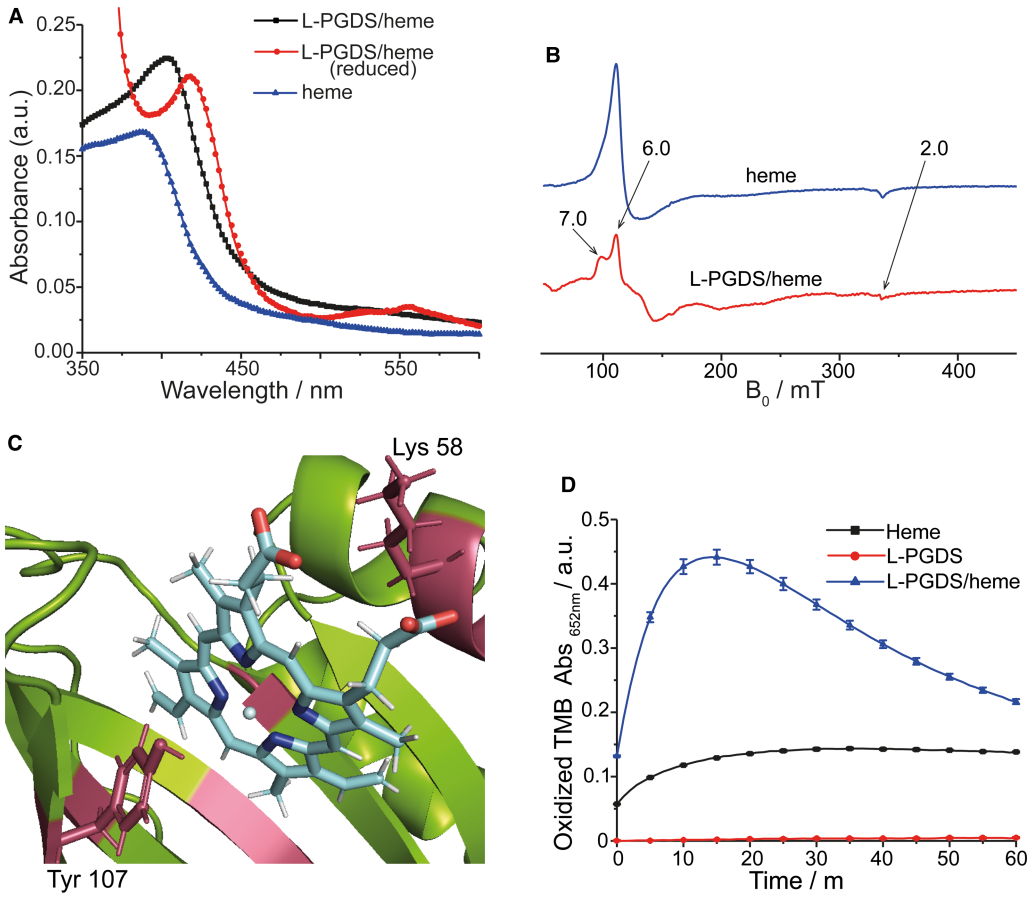


**Figure 1. Heme interaction with human WT L-PGDS.**

(**A**) UV/Vis absorption spectrum of heme binding to human WT L-PGDS. A Redshift of the Soret band of free heme occurring at 390 nm is observed when it binds to L-PGDS (404 nm). The addition of the reducing agent sodium dithionite results in a bathochromic shift of the L-PGDS/heme Soret band to 420 nm. (**B**) cw EPR spectra (9.3835 GHz) of L-PGDS/heme complex (mixed in a 1 : 1 molar ratio) recorded at 7.5 K. The Fe(III) signal observed around $g = 6.0$ indicates that heme is bound to WT L-PGDS in predominantly a high-spin, hexa-co-ordinate state. (**C**) Molecular Dynamics simulation model. A representative binding mode of heme to L-PGDS was obtained via docking to L-PGDS using HADDOCK followed by MD simulations and geometric clustering. Residues undergoing significant chemical shift perturbations or peak disappearance during NMR titration have been highlighted and mapped onto the crystal structure of WT L-PGDS (PDB:4 IMN). As observed from the model residues tyrosine 107 seems to be in proximity with the Fe atom in heme while the Lysine 58 side chain is close to the propionic groups in the heme moiety. (**D**) Peroxidase activity of WT L-PGDS/heme (in 1 : 1 molar ratio) was monitored by plotting the increase in absorbance at 652 nm for the oxidized TMB substrate versus time. Oxidation of the substrate by WT L-PGDS alone is negligible indicating that the peroxidase activity is due to heme binding to WT L-PGDS. A fast increase in the absorbance signal followed by a decrease in the signal intensity could possibly arise due to a fast rate of TMB oxidation by the L-PGDS/heme complex.

Since L-PGDS has a hexahistidine tag at the C terminus, we checked the binding of a synthetic, hexahistidine peptide with heme. The UV/Vis spectra (Supplementary Figure S3) showed no significant difference between free heme and the His-peptide-heme sample thus confirming that the histidine-tag alone cannot bind heme and is thus not involved in the heme interaction for the L-PGDS–heme complex.

The presence of hexa-co-ordinate, high-spin, Fe (III) heme was further supported by the X-band continuous wave EPR (cw EPR) spectrum of L-PGDS/heme in a 1 : 1 molar ratio complex (Figure 1B). The occurrence of a strong signal ∼120 mT (or $g_{\perp} = 6$) indicates high-spin heme where Fe(III) is hexa-co-ordinated with a proximal ligand from L-PGDS and a weak distal ligand, probably $H_2O$ [61,62]. The cw EPR spectrum of L-PGDS is

similar to spectra observed for many globin proteins where the heme Fe(III) paramagnetic center is hexa-co-ordinated, high-spin and in an environment with rhombic symmetry (intense signal at $g = 6$ with a shoulder at $g \sim 7$) [61,62].

To characterize the residues in WT L-PGDS involved in the interaction with the heme moiety, we performed an NMR titration of $^{15}N$ labeled, refolded, human WT L-PGDS with increasing concentration of heme. The 2D $^{1}H$–$^{15}N$ HSQC spectrum of L-PGDS was recorded in the presence and absence of heme and the assigned cross-peaks were monitored for changes in signal intensity or chemical shift perturbation upon interaction with heme at each titration step (Supplementary Figure S4). Several resonances (Supplementary Table S1) were significantly broadened presumably due to the strong paramagnetic relaxation induced by heme even at a lower protein to heme stoichiometry of 1 : 0.4, e.g. L-PGDS 150 μM: heme 60 μM (Supplementary Table S1). The broadened resonances of residues Lys 58, Lys 59, Tyr 107, Leu 131 and perturbed cross-peak of Met 145 present on the alpha-helix covering the entrance as well as lining the inner surface of the β-barrel lumen (Figure 1C, Supplementary Figure S5) is an indication that heme is positioned within L-PGDS potentially retaining some conformational mobility inside the lumen or exhibiting alternative orientations. We posit that these residues in L-PGDS are involved in direct interaction with heme undergoing conformational changes to adjust to the different orientations of the bound heme molecule thus leading to a more distributed cross-peak broadening. Similar observations have been reported earlier for the heme metabolite biliverdin binding to L-PGDS [4,5]. NMR titration data demonstrates L-PGDS/heme interactions are mostly hydrophobic in nature with Fe(III) heme axial coordination of Tyr 107 within the β-barrel cavity and the Lys 58 and Lys 59 most likely involved in direct interaction with the propionic acid side chains on the heme molecule. This interpretation is based on a significant broadening of resonances adjacent to Tyr 107 in early NMR titration steps as well as the high-spin rhombic heme observed in cw EPR spectra (intense signal at $g = 6$ with shoulders at $g = 7$). This type of coordination by a Tyr residue has also been found in previously reported cw EPR studies of several globin protein mutants (with the mutation to a tyrosine residue) [63–66].

Since in our extensive attempts to determine the 3D structure of the heme–L-PGDS complex by X-Ray crystallography no electron density attributable to heme was found in an otherwise highly resolved 1.5 A L-PGDS scaffold, we turned to computational methods in order to structurally explore the heme protein complex. The residues exhibiting broadened cross-peaks in NMR spectra were mapped onto the crystal structure of human WT L-PGDS (PDB: 4IMN) and HADDOCK was used to guide the docking of the heme moiety to L-PGDS (Supplementary Figure S5). MD simulation and geometric clustering (see Methods section) generated a representative conformation of the binding between L-PGDS and heme (Figure 1C). To evaluate the quality of our model, we generated a Ramachandran plot for L-PGDS residues of the representative model in the L-PGDS–heme complex using the Wincoot [67] software (Supplementary Figure S6, top panel). In the Ramachandran plot, 97.6% of the residues are preferred and allowed regions. When we checked the outlier residues, they were found to be in the loop regions of L-PGDS protein. Moreover, we calculated the RMSD of the L-PGDS–heme complex for 100 ns over three simulation repeats (Supplementary Figure S6, bottom panel). The RMSD of the complex was shown to be stable over simulation time.

Hydrogen peroxide ($H_2O_2$) which is one of the major components of ROS can be used for monitoring oxidative stress and cell-induced apoptosis [68–70]. The interaction of iron with hydrogen peroxide results in ROS [71]. We monitored the peroxidase activity of L-PGDS/heme complex by monitoring the increase in absorbance at 652 nm arising from the oxidation of TMB, a commonly used chromogenic substrate with a fixed concentration of hydrogen peroxide (Figure 1D). No peroxidase activity was observed for L-PGDS alone. This is supported by previously published results highlighting the role of L-PGDS in protection against oxidative-stress [42]. Interestingly, strong peroxidase activity was observed for the L-PGDS/heme complex due to heme binding. This is reflected in its ability to oxidize the substrate more efficiently than heme alone or L-PGDS alone. The sharp increase in the absorbance for oxidized TMB followed by a decrease in intensity of the oxidized substrate is characteristic of a fast-catalytic reaction. This high peroxidase activity of the L-PGDS/heme complex can be attributed to its hexa-co-ordinated heme molecule with axial coordination from a weak ligand at the distal position, rendering heme more accessible to the substrate (hydrogen peroxide) for oxidation. This proposed heme coordination to L-PGDS is further supported by the observation that addition of imidazole to the pre-formed L-PGDS/heme complex results in the redshift of the Soret band (Supplementary Figure S7) indicating that imidazole occupies the distal axial site for the Fe atom in heme after displacing the weak ligand (most likely water molecule). Interestingly, the organic substrate-TMB shows direct interaction with L-PGDS. Our ITC data confirms that TMB binds to the WT L-PGDS with an apparent binding constant $K_d = 15$ μM

Biochemical Journal (2020) 477 1227–1240
https://doi.org/10.1042/BCJ20190536

using a sequential fit binding site model (Supplementary Figure S8). Due to the binding of the substrate itself to L-PGDS, we hypothesize that any ROS that is released via the breakdown of the more toxic $H_2O_2$ will bind to the substrate that is in complex with L-PGDS instead of being released into the environment as free ROS species.

L-PGDS, the second most abundant chaperone in human CSF, has also been reported to bind heme metabolites with high affinity thus acting as a scavenger in the human brain [1,2,8,72]. The levels of bilirubin and its derivatives were found to be high in the CSF in AD patients [22] and speculated to affect the chaperone activity of L-PGDS by binding to it. Thus, to further investigate L-PGDS chaperone activity in the presence of heme metabolites, ThT assay was performed to study inhibition of Aβ(1–40) and Aβ(25–35) peptides aggregation in the presence of refolded, human WT L-PGDS in complex with bilirubin. Aβ(25–35) peptide derived from the full-length Aβ42 is known to have high aggregation and neurotoxic properties [73] and was therefore selected for the L-PGDS chaperone functional assay. Since heme itself has been shown to prevent aggregation of Aβ by binding to its monomers [74,75], the presence of heme in the assay could potentially mask the chaperone activity of WT L-PGDS. This was another reason we opted for bilirubin instead which is a by-product of heme metabolism and has been shown to bind to L-PGDS with equally high affinity [2] and similarity as heme, for the ThT assay. The binding of bilirubin to L-PGDS was determined spectrophotometrically where L-PGDS binding to bilirubin was detected as a redshift in the Soret band when compared with free bilirubin (Supplementary Figure S9). This L-PGDS–bilirubin complex was then used for the following ThT assay for monitoring the inhibition of Aβ(1–40) and Aβ(25–35) peptide aggregation. Figure 2A,B shows distinct sigmoidal curves characteristic of Aβ(1–40) and Aβ(25–35) fibril formation in 20 h and 10 h, respectively [76]. In the presence of L-PGDS alone, the fluorescence intensity of Aβ(1–40) and Aβ(25–35) fibrils was considerably reduced as compared with the Aβ fibril controls, indicating effective inhibition of Aβ fibril elongation. Remarkably, the presence of bilirubin in complex with L-PGDS did not significantly affect L-PGDS chaperone activity as the L-PGDS–bilirubin complex showed equal efficiency in inhibiting the Aβ(1–40) and Aβ(25–35) fibril elongation (Figure 2A,B). The ability to bind to the heme metabolite bilirubin while effectively inhibiting the aggregation of Aβ(1–40) and Aβ(25–35) peptides (Figure 2C) confirms (1) that there is no competitive binding between the two high-affinity binders — amyloid β peptide and bilirubin and (2) the presence of heme or heme-metabolite does not affect WT L-PGDS chaperone function. To further visualize the formation of this ternary complex, bilirubin was docked to L-PGDS and the complex was aligned to a representative model of WT L-PGDS in complex with Aβ(1–40) as the starting scaffold (Kannaian et al. [43]), to which MD simulations and geometric clustering were performed (Figure 2D).

The complex formation between L-PGDS/heme/Aβ peptide was further investigated by monitoring the UV/Vis absorption spectroscopy of heme binding to Aβ(1–40) and Aβ(1–16) peptides, both of which contain the heme coordinating residues His 6, Tyr 10, His 13 and His 14 [20]. Heme bound to Aβ(1–16) and Aβ(1–40) peptides was confirmed by a redshift of the Soret band of free heme from 390 nm to 412 nm with low-intensity α, β bands in the 500–600 nm range, similar to that reported previously [20] (Figure 3). The Aβ(25–35) peptide does not contain the heme binding motif hence did not show any characteristic Soret band for the Aβ (25–35)/heme complex (Supplementary Figure S10). Interestingly, the addition of refolded L-PGDS to the preformed Aβ(1–16)/heme or Aβ(1–40)/heme complex results in a shift of the existing Soret band of Aβ/heme complex at 412 nm to the position characteristic of L-PGDS/heme complex at 404 nm (Figure 3A,B). This shift is indicative of the ability of L-PGDS to extract the heme which is bound to Aβ peptide. The displacement is more distinct for Aβ(1–16) (Figure 3A) possibly due to the higher affinity of L-PGDS for heme, ∼38 nM as compared with ∼120 nM previously reported for Aβ(1–16)/heme. The subtle change in the low-intensity α, β bands within 500–600 nm range for the Aβ(1–40)/heme upon addition of L-PGDS (Figure 3B) also indicates a change in the heme environment which can be attributed to binding with L-PGDS.

Peroxidase activity of the Aβ(1–40)/heme complex in the presence of WT L-PGDS was studied by monitoring the increase in absorbance at 652 nm of the organic substrate TMB over a period of 1 h (Figure 4). As reported earlier, the Aβ(1–40)/heme complex showed a high peroxidase activity compared with the negligible activity of the monomeric Aβ(1–40) peptide alone. Interestingly, the addition of WT L-PGDS to the preformed Aβ(1–40)/heme complex resulted in a sharp increase in the absorbance at 652 nm implying faster oxidation of the substrate which is similar to L-PGDS/heme complex. Since WT L-PGDS alone does not show any peroxidase activity (Figure 1D), the increase in substrate oxidation upon addition of L-PGDS to Aβ/heme complex can be explained when considering the ability of WT L-PGDS to efficiently extract heme from the preformed Aβ40/heme complex to now form the L-PGDS/heme complex. In its new environment, the heme

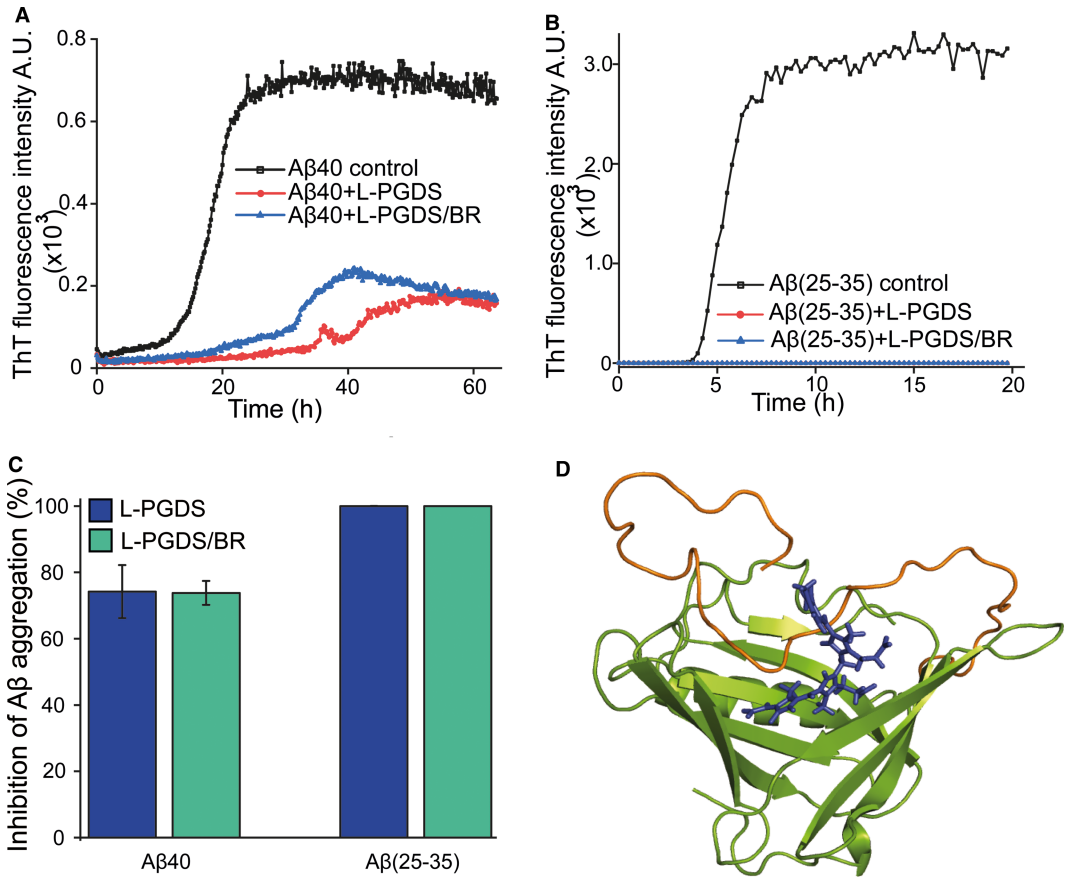


**Figure 2. Amyloid β chaperone activity of L-PGDS in complex with heme metabolite–bilirubin.**

(**A**) ThT curve for WT L-PGDS in the presence and absence of bilirubin (blue and red, respectively) showing similar inhibition of Aβ(1–40) peptide aggregation. The black curve is an Aβ(1–40) peptide control showing fibril formation after 20 h. (**B**) ThT assay was done for Aβ(25–35) peptide showing fibril formation of the peptide alone within 10 h. The presence of bilirubin in complex with WT L-PGDS does not affect its ability to inhibit Aβ(25–35) aggregation. (**C**) Overall chaperone activity of WT L-PGDS plotted for Aβ(1–40) and Aβ(25–35) peptides in the presence and absence of bilirubin. (**D**) Model of human WT L-PGDS in complex with the heme metabolite bilirubin and Aβ(1–40) peptide. L-PGDS crystal structure (PDB:4imn) is shown in green with bilirubin (blue) residing in the lipocalin cavity and the Aβ peptide (orange) binds at the top of the lipocalin calyx. The model was obtained after docking bilirubin to L-PGDS using the HADDOCK web server and aligning the model to the complex of the L-PGDS–Aβ(1–40). The co-ordinates of L-PGDS, Aβ(1–40) and bilirubin were extracted and subjected to molecular dynamics (MD) simulation and geometric clustering.

molecule is hexa-co-ordinated with a weak ligand at the distal coordination site which can be easily replaced by the hydrogen peroxide molecule to further oxidize the substrate TMB.

# Discussion

Lipocalin-type prostaglandin is a scavenger of heme and heme metabolites, bilirubin and biliverdin. Refolded WT L-PGDS binding heme in a 1 : 1 stoichiometry and with high affinity was confirmed by the combined results from UV/Vis, cw EPR, Tryptophan Quenching and solution NMR studies. As apparent from UV/Vis absorption data, heme binding to WT L-PGDS was established as a bathochromic shift (15 nm), increase in signal intensity and change in the shape of the absorption Soret band when compared with free heme. A strong signal around $g_{\perp} = 6$ in the cw EPR spectrum confirms the high-spin state of the Fe(III) of the heme molecule. Intrinsic tryptophan quenching data analysis indicated heme molecule present in the lipocalin cavity such that it is in proximity (within 15 Å) to all three tryptophan residues (W 43, W 54 and W 112) to cause complete quenching of tryptophan fluorescence intensity. Solution-state NMR titration data displayed

*Biochemical Journal* (2020) **477** 1227–1240
https://doi.org/10.1042/BCJ20190536

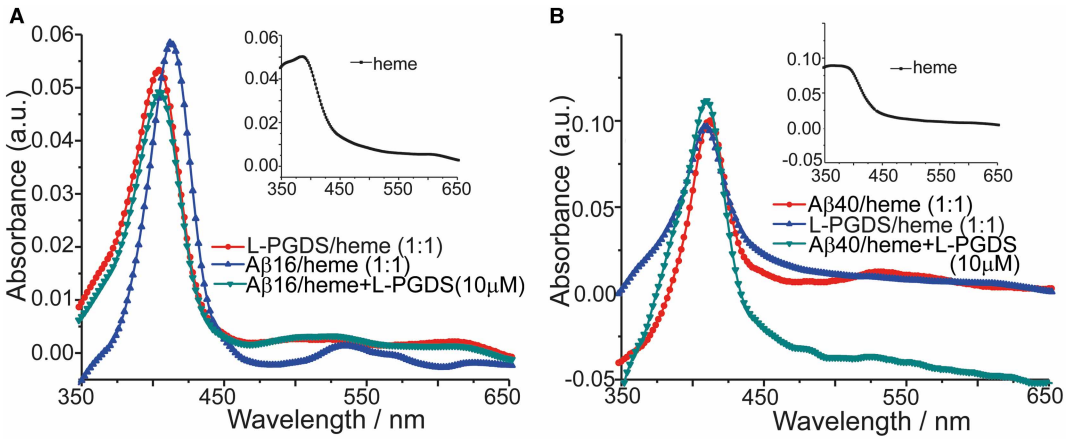


**Figure 3. UV/Vis absorption spectra of WT L-PGDS interaction with pre-formed Aβ/heme complex.**

(**A**) Absorption spectra of Aβ16 in complex with heme (1 : 1: molar ratio) show characteristic Soret band at >420 nm and two small α, β band within 500–600 nm range characteristic of bis-histidine coordination. The addition of WT L-PGDS shifts the Soret band to a position similar to L-PGDS/heme complex. Free heme shows a broad peak between 38 and 390 nm. (**B**) Absorption spectra Aβ40 with heme in a 1 : 1 molar ratio showing Soret band at 418 nm and small α, β band within 500–600 nm range indicative of Aβ/heme complex formation. The addition of WT L-PGDS shifts the Soret peak to L-PGDS/heme complex and the change is more pronounced in the 500–600 nm range with reduced intensity of the previously visible α, β bands. Heme spectra are shown in the inset.

widespread signal disappearance of several residues of WT L-PGDS upon heme addition. These residues reside within the β barrel, helix and EF-loop of the L-PGDS protein. The side chain of Tyr 107 is most likely involved in axial coordination with the Fe of heme while Lys 58 and Lys 59 are involved in direct interaction with the non-pyrrole side chains of the heme molecule while the side chain of Met 145 is most likely involved in direct linkage with heme. Similar interactions between residues such as Lysine, tyrosine and methionine have been previously reported for human alpha-microglobulin [77], mutants of many globin proteins [63–66] and human myeloperoxidases [78]. Human L-PGDS acts as a ROS scavenger by binding the ROS released from $H_2O_2$ breakdown. This happens because of oxidation of the Cys 65 thiol group to sulfinic acid [42]. The L-PGDS/heme interaction is an important function meant to scavenge heme and heme metabolites in the CSF of human patients after stroke or in cancer [79] or even in patients with aneurysmal subarachnoid hemorrhage

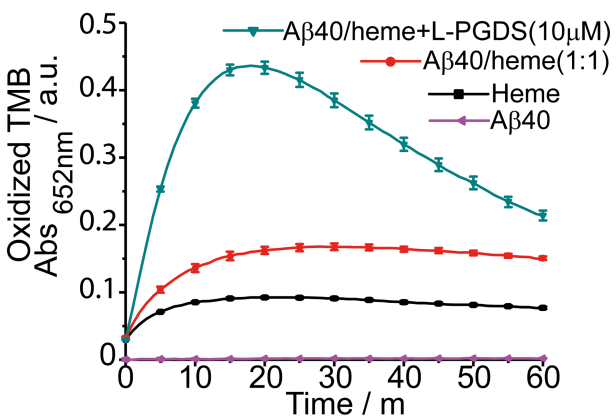


**Figure 4. Peroxidase Activity of L-PGDS with pre-formed Aβ/heme complex.**

Aβ(1–40)/heme complex shows peroxidase activity as seen by an increase in the absorbance at 652 nm for the oxidized TMB substrate. Oxidation of TMB by monomeric Aβ(1–40) peptide alone is negligible indicating that oxidation of the substrate cannot happen in the absence of heme. The peroxidase activity was monitored for 1 h.

(SAH) [80]. It was also reported that high levels of L-PGDS are present in the CSF after SAH and that L-PGDS 'scavenges' hemoglobin metabolite — biliverdin thus involved in clearance of the toxic lipophilic molecules [72]. However, L-PGDS when in complex with heme also behaves as a peroxidase as demonstrated by our peroxidase assay. SAH is known to induce neuronal injures due to the accumulation of free heme released from damaged erythrocytes [81]. It is, therefore, reasonable to assume that after SAH, where there is an increased level of L-PGDS in the CSF along with increased amounts of free heme, there is a high possibility that increased levels of L-PGDS/heme complex react with endogenous hydrogen peroxide (released due to auto-oxidation of oxyhemoglobin [82]) thus generating high levels of ROS. This is further supported by direct evidence for the formation of reactive oxidative species, especially superoxide anion, in the subarachnoid space after SAH [83]. In AD pathology, it has been reported that gradual breakdown of small blood vessels in the brain leads to the accumulation of high levels of free heme in the brain tissue as the disease progresses [84]. Thus, with increasing levels of hydrogen peroxide (produced by activation of immune cells like astrocyte) and higher levels of L-PGDS/heme complex the increased peroxidase activity of the complex may increase the oxidative stress on the neuronal cells.

L-PGDS as a multifunctional enzyme with a broad-range ligand binding selectivity [1,3] also shows binding to the substrate TMB (Supplementary Figure S9). Thus, it is also reasonable to assume that ROS released by the breakdown of $H_2O_2$ by the peroxidase activity of the L-PGDS/heme complex, is captured by the oxidation of TMB, a substrate which is likely bound to L-PGDS. Thus, instead of being released in the environment, L-PGDS may be useful in reducing high levels of toxic $H_2O_2$ by channeling it to towards specific substrate targets bound to L-PGDS itself (such as TMB in this case). In contrast, amyloid β induces accumulation of high levels of $H_2O_2$ and lipid peroxides in the cell [26] and upon binding to metal ions such as heme acts as a peroxidase, further increasing the oxidative stress on the cell [20,23,74].

Our UV/Vis spectrometry data demonstrates the ability of WT L-PGDS to extract heme from the pre-formed Aβ/heme complex. The resulting complex exhibits similar peroxidase activity as L-PGDS/heme. Unlike L-PGDS/heme, Aβ/heme complex cannot accommodate any other substrate hence it is incapable of limiting highly toxic free ROS in the cellular environment. Thus, we posit that when L-PGDS extracts heme from Aβ/heme complex, *in vitro*, it plays a protective role by limiting the release of free ROS in the cellular environment. The oxidation of the substrate bound to L-PGDS/heme complex will thus prevent the non-selective and uncontrolled oxidative damage that Aβ/heme complex can generate.

# Conclusion

In this paper, we confirm the high-affinity binding of heme to recombinant human WT L-PGDS with the heme moiety present in a high-spin Fe(III) state. The presence of high-spin heme is further supported by the high peroxidase activity of the L-PGDS/heme complex. The 'pseudo-peroxidase' nature of the L-PGDS/heme complex has been reported here for the first time. We postulate that at physiologically relevant concentrations, L-PGDS/heme complex can use $H_2O_2$ as a substrate to break it down to ROS which gets 'trapped' by the self-oxidizing second substrate bound to L-PGDS resulting in effective reduction in $H_2O_2$ concentrations in its native environment. We also report for the first time the amyloid β chaperone activity of L-PGDS/bilirubin complex, demonstrating that L-PGDS maintains its 'scavenger' property while effectively inhibiting Aβ peptide aggregation. As a consequence of its higher affinity for heme than amyloid β peptide, the addition of WT L-PGDS to pre-formed Aβ/heme complex might help in reducing oxidative damage. As evident from our data, L-PGDS can extract the heme from a pre-formed Aβ/heme complex; this L-PGDS/heme complex is more likely to breakdown the more harmful $H_2O_2$ into the less harmful oxidized substrate while protecting cells from free ROS. Overall our findings reinforce the possible neuroprotective role of WT L-PGDS in conditions such as AD which are characterized by increased Aβ aggregates which increase the levels of hydrogen peroxide in the cellular environment as well as the Aβ/heme complex which triggers the buildup of free ROS leading to oxidative-stress mediated cellular apoptosis.

### Abbreviations

AD, Alzheimer's disease; CSF, cerebrospinal fluid; EPR, electron paramagnetic resonance; GSSG, getting oxidized to its disulfide form; L-PGDS, lipocalin-type prostaglandin D synthase; RMSD, root mean square deviation; SAH, subarachnoid hemorrhage.

*Biochemical Journal* (2020) **477** 1227–1240
https://doi.org/10.1042/BCJ20190536

## Acknowledgement

The research for this paper was supported by the MOE-Tier 2 grant M4020231. J.R.H. acknowledges support from the ARC (FT120100421).

## Author Contribution

M.P. performed and analyzed data from UV/Vis, NMR and Peroxidase assay and wrote the manuscript. B.K. prepared the L-PGDS protein sample and performed and analyzed the ThT assay. J.Y. and M.Y. performed the heme docking and MD simulation. R.K. and J.R.H. performed and analyzed the EPR data. KP supervised the project. All authors contributed to editing the manuscript.

## Competing Interests

The authors declare that there are no competing interests associated with the manuscript.

# References

1 Kume, S., Lee, Y.H., Nakatsuji, M., Teraoka, Y., Yamaguchi, K., Goto, Y. et al. (2014) Fine-tuned broad binding capability of human lipocalin-type prostaglandin D synthase for various small lipophilic ligands. *FEBS Lett.* **588**, 962–969 https://doi.org/10.1016/j.febslet.2014.02.001

2 Kume, S., Lee, Y.H., Miyamoto, Y., Fukada, H., Goto, Y. and Inui, T. (2012) Systematic interaction analysis of human lipocalin-type prostaglandin D synthase with small lipophilic ligands. *Biochem. J.* **446**, 279–289 https://doi.org/10.1042/BJ20120324

3 Teraoka, Y., Kume, S., Lin, Y., Atsuji, S. and Inui, T. (2017) Comprehensive evaluation of the binding of lipocalin-type prostaglandin D synthase to poorly water-soluble drugs. *Mol. Pharm.* **14**, 3558–3567 https://doi.org/10.1021/acs.molpharmaceut.7b00590

4 Miyamoto, Y., Nishimura, S., Inoue, K., Shimamoto, S., Yoshida, T., Fukuhara, A. et al. (2010) Structural analysis of lipocalin-type prostaglandin D synthase complexed with biliverdin by small-angle X-ray scattering and multi-dimensional NMR. *J. Struct. Biol.* **169**, 209–218 https://doi.org/10.1016/j.jsb.2009.10.005

5 Inoue, K., Yagi, N., Urade, Y. and Inui, T. (2009) Compact packing of lipocalin-type prostaglandin D synthase induced by binding of lipophilic ligands. *J. Biochem.* **145**, 169–175 https://doi.org/10.1093/jb/mvn154

6 Lescuyer, P., Gandini, A., Burkhard, P.R., Hochstrasser, D.F. and Sanchez, J.C. (2005) Prostaglandin D2 synthase and its post-translational modifications in neurological disorders. *Electrophoresis* **26**, 4563–4570 https://doi.org/10.1002/elps.200500292

7 Qu, W.-M., Huang, Z.L., Xu, X.H., Aritake, K., Eguchi, N., Nambu, F. et al. (2006) Lipocalin-type prostaglandin D synthase produces prostaglandin D2 involved in regulation of physiological sleep. *Proc. Natl. Acad. Sci. U.S.A.* **103**, 17949–17954 https://doi.org/10.1073/pnas.0608581103

8 Kanekiyo, T., Ban, T., Aritake, K., Huang, Z.L., Qu, W.M., Okazaki, I. et al. (2007) Lipocalin-type prostaglandin D synthase/beta-trace is a major amyloid beta-chaperone in human cerebrospinal fluid. *Proc. Natl. Acad. Sci. U.S.A.* **104**, 6412–6417 https://doi.org/10.1073/pnas.0701585104

9 Khoonsari, P.E., Häggmark, A., Lönnberg, M., Mikus, M., Kilander, L., Lannfelt, L. et al. (2016) Analysis of the cerebrospinal fluid proteome in Alzheimer's disease. *PLoS One* **11**, e0150672 https://doi.org/10.1371/journal.pone.0150672

10 Zhang, Q., Ma, C., Gearing, M., Wang, P.G., Chin, L.S. and Li, L. (2018) Integrated proteomics and network analysis identifies protein hubs and network alterations in Alzheimer's disease. *Acta Neuropathol. Commun.* **6**, 19 https://doi.org/10.1186/s40478-018-0524-2

11 Seyfried, N.T., Dammer, E.B., Swarup, V., Nandakumar, D., Duong, D.M., Yin, L. et al. (2017) A multi-network approach identifies protein-specific co-expression in asymptomatic and symptomatic Alzheimer's disease. *Cell Syst.* **4**, 60–72.e4 https://doi.org/10.1016/j.cels.2016.11.006

12 Klementieva, O., Willén, K., Martinsson, I., Israelsson, B., Engdahl, A., Cladera, J. et al. (2017) Pre-plaque conformational changes in Alzheimer's disease-linked abeta and APP. *Nat. Commun.* **8**, 14726 https://doi.org/10.1038/ncomms14726

13 Ashraf, G.M., Greig, N.H., Khan, T.A., Hassan, I., Tabrez, S., Shakil, S. et al. (2014) Protein misfolding and aggregation in Alzheimer's disease and type 2 diabetes mellitus. *CNS Neurol. Disord. Drug Targets* **13**, 1280–1293 https://doi.org/10.2174/1871527313666140917095514

14 Huang, X., Mariana A, C.S.A., Hartshorn, G.M., Goldstein, L.E., Scarpa, R.C., Cuajungco, M.P. et al. (1999) The Aβ peptide of Alzheimer's disease directly produces hydrogen peroxide through metal ion reduction. *Biochemistry* **38**, 7609–7616 https://doi.org/10.1021/bi990438f

15 Pramanik, D., Ghosh, C. and Dey, S.G. (2011) Heme-Cu bound abeta peptides: spectroscopic characterization, reactivity, and relevance to Alzheimer's disease. *J. Am. Chem. Soc.* **133**, 15545–15552 https://doi.org/10.1021/ja204628b

16 Pramanik, D., Ghosh, C., Mukherjee, S. and Dey, S.G. (2013) Interaction of amyloid β peptides with redox active heme cofactor: relevance to Alzheimer's disease. *Coord. Chem. Rev.* **257**, 81–92 https://doi.org/10.1016/j.ccr.2012.02.025

17 Sayre, L.M., Zelasko, D.A., Harris, P.L., Perry, G., Salomon, R.G. and Smith, M.A. (1997) 4-Hydroxynonenal-derived advanced lipid peroxidation end products are increased in Alzheimer's disease. *J. Neurochem.* **68**, 2092–2097 https://doi.org/10.1046/j.1471-4159.1997.68052092.x

18 Smith, D.G., Cappai, R. and Barnham, K.J. (2007) The redox chemistry of the Alzheimer's disease amyloid beta peptide. *Biochim. Biophys. Acta* **1768**, 1976–1990 https://doi.org/10.1016/j.bbamem.2007.02.002

19 Huang, X., Moir, R.D., Tanzi, R.E., Bush, A.I. and Rogers, J.T. (2004) Redox-active metals, oxidative stress, and Alzheimer's disease pathology. *Ann. NY Acad. Sci.* **1012**, 153–164 https://doi.org/10.1196/annals.1306.012

20 Atamna, H. and Frey, II, W.H. (2004) A role for heme in Alzheimer's disease: heme binds amyloid beta and has altered metabolism. *Proc. Natl. Acad. Sci. U.S.A.* **101**, 11153–11158 https://doi.org/10.1073/pnas.0404349101

21 Wagner, K.R., Sharp, F.R., Ardizzone, T.D., Lu, A. and Clark, J.F. (2003) Heme and iron metabolism: role in cerebral hemorrhage. *J. Cereb. Blood Flow Metab.* **23**, 629–652 https://doi.org/10.1097/01.WCB.0000073905.87928.6D

22 Kimpara, T., Takeda, A., Yamaguchi, T., Arai, H., Okita, N., Takase, S. et al. (2000) Increased bilirubins and their derivatives in cerebrospinal fluid in Alzheimer's disease. *Neurobiol. Aging* **21**, 551–554 https://doi.org/10.1016/S0197-4580(00)00128-7

23 Atamna, H. and Boyle, K. (2006) Amyloid-beta peptide binds with heme to form a peroxidase: relationship to the cytopathologies of Alzheimer's disease. *Proc. Natl. Acad. Sci. U.S.A.* **103**, 3381–3386 https://doi.org/10.1073/pnas.0600134103

24 Fridovich, I. (1978) The biology of oxygen radicals. *Science* **201**, 875–880 https://doi.org/10.1126/science.210504
25 Armstrong, D. (1984) *Free Radicals in Molecular Biology, Aging, and Disease*, vol. **xv**, 416 p, Raven Press, New York
26 Behl, C., Davis, J.B., Lesley, R. and Schubert, D. (1994) Hydrogen peroxide mediates amyloid beta protein toxicity. *Cell* **77**, 817–827 https://doi.org/10.1016/0092-8674(94)90131-7
27 Hassan, H.M. (1988) Biosynthesis and regulation of superoxide dismutases. *Free Radic. Biol. Med.* **5**, 377–385 https://doi.org/10.1016/0891-5849(88)90111-6
28 Clement, M.V., Ponton, A. and Pervaiz, S. (1998) Apoptosis induced by hydrogen peroxide is mediated by decreased superoxide anion concentration and reduction of intracellular milieu. *FEBS Lett.* **440**, 13–18 https://doi.org/10.1016/S0014-5793(98)01410-0
29 Southorn, P.A. and Powis, G. (1988) Free radicals in medicine. I. chemical nature and biologic reactions. *Mayo Clin. Proc.* **63**, 381–389 https://doi.org/10.1016/S0025-6196(12)64861-7
30 Burdon, R.H. (1995) Superoxide and hydrogen peroxide in relation to mammalian cell proliferation. *Free Radic. Biol. Med.* **18**, 775–794 https://doi.org/10.1016/0891-5849(94)00198-S
31 Burdon, R.H. (1996) Control of cell proliferation by reactive oxygen species. *Biochem. Soc. Trans.* **24**, 1028–1032 https://doi.org/10.1042/bst0241028
32 Pervaiz, S., Ramalingam, J.K., Hirpara, J.L. and Clement, M.V. (1999) Superoxide anion inhibits drug-induced tumor cell death. *FEBS Lett.* **459**, 343–348 https://doi.org/10.1016/S0014-5793(99)01258-2
33 Clement, M.V. and Pervaiz, S. (1999) Reactive oxygen intermediates regulate cellular response to apoptotic stimuli: an hypothesis. *Free Radic. Res.* **30**, 247–252 https://doi.org/10.1080/10715769900300271
34 Pervaiz, S. and Clement, M.V. (2002) A permissive apoptotic environment: function of a decrease in intracellular superoxide anion and cytosolic acidification. *Biochem. Biophys. Res. Commun.* **290**, 1145–1150 https://doi.org/10.1006/bbrc.2001.6274
35 Pervaiz, S. and Clement, M.V. (2002) Hydrogen peroxide-induced apoptosis: oxidative or reductive stress? *Methods Enzymol.* **352**, 150–159 https://doi.org/10.1016/S0076-6879(02)52015-2
36 Hirpara, J.L., Clement, M.V. and Pervaiz, S. (2001) Intracellular acidification triggered by mitochondrial-derived hydrogen peroxide is an effector mechanism for drug-induced apoptosis in tumor cells. *J. Biol. Chem.* **276**, 514–521 https://doi.org/10.1074/jbc.M004687200
37 Clement, M.V. and Pervaiz, S. (2001) Intracellular superoxide and hydrogen peroxide concentrations: a critical balance that determines survival or death. *Redox Rep.* **6**, 211–214 https://doi.org/10.1179/135100001101536346
38 Cao, C., Leng, Y. and Kufe, D. (2003) Catalase activity is regulated by c-Abl and Arg in the oxidative stress response. *J. Biol. Chem.* **278**, 29667–29675 https://doi.org/10.1074/jbc.M301292200
39 Day, B.J. (2009) Catalase and glutathione peroxidase mimics. *Biochem. Pharmacol.* **77**, 285–296 https://doi.org/10.1016/j.bcp.2008.09.029
40 Djordjevic, V.B. (2004) Free radicals in cell biology. *Int. Rev. Cytol.* **237**, 57–89 https://doi.org/10.1016/S0074-7696(04)37002-6
41 Chatterjee, S., Jungraithmayr, W. and Bagchi, D. (2017) *Immunity and Inflammation in Health and Disease: Emerging Roles of Nutraceuticals and Functional Foods in Immune Support*, Academic Press, Elsevier
42 Fukuhara, A., Yamada, M., Fujimori, K., Miyamoto, Y., Kusumoto, T., Nakajima, H. et al. (2012) Lipocalin-type prostaglandin D synthase protects against oxidative stress-induced neuronal cell death. *Biochem. J.* **443**, 75–84 https://doi.org/10.1042/BJ20111889
43 Kannaian, B., Sharma, B., Phillips, M., Chowdhury, A., Manimekalai, M.S.S., Adav, S.S. et al. (2019) Abundant neuroprotective chaperone lipocalin-type prostaglandin D synthase (L-PGDS) disassembles the amyloid-beta fibrils. *Sci. Rep.* **9**, 12579 https://doi.org/10.1038/s41598-019-48819-5
44 Zhou, Y., Shaw, N., Li, Y., Zhao, Y., Zhang, R. and Liu, Z.J. (2010) Structure-function analysis of human l-prostaglandin D synthase bound with fatty acid molecules. *FASEB J.* **24**, 4668–4677 https://doi.org/10.1096/fj.10-164863
45 D'Souza, A., Wu, X., Yeow, E.K.L. and Bhattacharjya, S. (2017) Designed heme-cage β-sheet miniproteins. *Angew. Chem.* **129**, 5998–6002 https://doi.org/10.1002/ange.201702472
46 D'Souza, A., Mahajan, M. and Bhattacharjya, S. (2016) Designed multi-stranded heme binding β-sheet peptides in membrane. *Chem. Sci.* **7**, 2563–2571 https://doi.org/10.1039/C5SC04108B
47 Keller, R.L.J. (2011) The Computer Aided Resonance Assignment Tutorial.pdf. http://cara.nmr-software.org/downloads/3-85600-112-3.pdf
48 van Zundert, G.C.P., Rodrigues, J.P.G.L.M., Trellet, M., Schmitz, C., Kastritis, P.L., Karaca, E. et al. (2016) The HADDOCK2.2 webserver: User-friendly integrative modeling of biomolecular complexes. *J. Mol. Biol.* **428**, 720–725 https://doi.org/10.1016/j.jmb.2015.09.014
49 Berman, H.M., Westbrook, J., Feng, Z., Gilliland, G., Bhat, T.N., Weissig, H. et al. (2000) The protein data bank. *Nucleic Acids Res.* **28**, 235–242 https://doi.org/10.1093/nar/28.1.235
50 Lim, S.M., Chen, D., Teo, H., Roos, A., Jansson, A.E., Nyman, T. et al. (2013) Structural and dynamic insights into substrate binding and catalysis of human lipocalin prostaglandin D synthase. *J. Lipid Res.* **54**, 1630–1643 https://doi.org/10.1194/jlr.M035410
51 Van Der Spoel, D., Lindahl, E., Hess, B., Groenhof, G., Mark, A.E. and Berendsen, H.J. (2005) GROMACS: fast, flexible, and free. *J. Comput. Chem.* **26**, 1701–1718 https://doi.org/10.1002/jcc.20291
52 Huang, J., Rauscher, S., Nawrocki, G., Ran, T. and Feig, M. (2017) CHARMM36m: an improved force field for folded and intrinsically disordered proteins **14**, 71–73 PMID: 27819658
53 Jo, S., Kim, T., Iyer, V.G. and Im, W. (2008) CHARMM-GUI: a web-based graphical user interface for CHARMM. *J. Comput. Chem.* **29**, 1859–1865 https://doi.org/10.1002/jcc.20945
54 Jorgensen, W.L., Chandrasekhar, J., Madura, J.D., Impey, R.W. and Klein, M.L. (1983) Comparison of simple potential functions for simulating liquid water. *J. Chem. Phys.* **79**, 926–935 https://doi.org/10.1063/1.445869
55 Hess, B. (2008) P-LINCS: a parallel linear constraint solver for molecular simulation. *J. Chem. Theory Comput.* **4**, 116–122 https://doi.org/10.1021/ct700200b
56 Darden, T., York, D. and Pedersen, L. (1993) Particle mesh ewald: an N·log(N) method for ewald sums in large systems. *J. Chem. Phys.* **98**, 10089–10092 https://doi.org/10.1063/1.464397
57 Bussi, G., Donadio, D. and Parrinello, M. (2007) Canonical sampling through velocity rescaling. *J. Chem. Phys.* **126**, 014101 https://doi.org/10.1063/1.2408420
58 Rojas, N.R., Kamtekar, S., Simons, C.T., McLean, J.E., Vogel, K.M., Spiro, T.G. et al. (1997) De novo heme proteins from designed combinatorial libraries. *Protein Sci.* **6**, 2512–2524 https://doi.org/10.1002/pro.5560061204

*Biochemical Journal* (2020) **477** 1227–1240
https://doi.org/10.1042/BCJ20190536


59 Margoliash, E. (1991) Cytochromes-C - evolutionary, structural and physicochemical aspects - moore,Gr, pettigrew,Gw. *Science* **252**, 1001–1001 https://doi.org/10.1126/science.252.5008.1001

60 Antonini, E. and Brunori, M. (1971) *Hemoglobin and Myoglobin in Their Reactions with Ligands*, vol. **xx**, 436 p, North-Holland Pub. Co., Amsterdam

61 Flores, M., Wajnberg, E. and Bemski, G. (1997) Temperature dependence of Q-band electron paramagnetic resonance spectra of nitrosyl heme proteins. *Biophys J.* **73**, 3225–3229 https://doi.org/10.1016/S0006-3495(97)78347-4

62 Van Doorslaer, S. and Cuypers, B. (2018) Electron paramagnetic resonance of globin proteins - a successful match between spectroscopic development and protein research. *Mol. Phys.* **116**, 287–309 https://doi.org/10.1080/00268976.2017.1392629

63 Adachi, S., Nagano, S., Ishimori, K., Watanabe, Y., Morishima, I., Egawa, T. et al. (1993) Roles of proximal ligand in heme proteins: replacement of proximal histidine of human myoglobin with cysteine and tyrosine by site-directed mutagenesis as models for P-450, chloroperoxidase, and catalase. *Biochemistry* **32**, 241–252 https://doi.org/10.1021/bi00052a031

64 Egeberg, K.D., Springer, B.A., Martinis, S.A., Sligar, S.G., Morikis, D. and Champion, P.M. (1990) Alteration of sperm whale myoglobin heme axial ligation by site-directed mutagenesis. *Biochemistry* **29**, 9783–9791 https://doi.org/10.1021/bi00494a004

65 Williams-Smith, D.L. and Patel, K. (1975) Induced changes in the electron paramagnetic resonance spectra of mammalian catalases. *Biochim. Biophys. Acta* **405**, 243–252 https://doi.org/10.1016/0005-2795(75)90091-4

66 Nagai, M., Mawatari, K., Nagai, Y., Horita, S., Yoneyama, Y. and Hori, H. (1995) Studies of the oxidation states of hemoglobin M Boston and hemoglobin M saskatoon in blood by EPR spectroscopy. *Biochem. Biophys. Res. Commun.* **210**, 483–490 https://doi.org/10.1006/bbrc.1995.1686

67 Emsley, P., Lohkamp, B., Scott, W.G. and Cowtan, K. (2010) Features and development of coot. *Acta Crystallogr. D Biol. Crystallogr.* **66**, 486–501 https://doi.org/10.1107/S0907444910007493

68 Chaube, S.K., Prasad, P.V., Thakur, S.C. and Shrivastav, T.G. (2005) Hydrogen peroxide modulates meiotic cell cycle and induces morphological features characteristic of apoptosis in rat oocytes cultured in vitro. *Apoptosis* **10**, 863–874 https://doi.org/10.1007/s10495-005-0367-8

69 Miyazato, H., Taira, J. and Ueda, K. (2016) Hydrogen peroxide derived from marine peroxy sesquiterpenoids induces apoptosis in HCT116 human colon cancer cells. *Bioorg. Med. Chem. Lett.* **26**, 4641–4644 https://doi.org/10.1016/j.bmcl.2016.08.057

70 Lu, X., Kambe, F., Cao, X., Kozaki, Y., Kaji, T., Ishii, T. et al. (2008) 3 beta-hydroxysteroid-Delta 24 reductase is a hydrogen peroxide scavenger, protecting cells from oxidative stress-induced apoptosis. *Endocrinology* **149**, 3267–3273 https://doi.org/10.1210/en.2008-0024

71 Vlasova, I.I. (2018) Peroxidase activity of human hemoproteins: keeping the fire under control. *Molecules* **23**, E2561 https://doi.org/10.3390/molecules23102561

72 Inui, T., Mase, M., Shirota, R., Nagashima, M., Okada, T. and Urade, Y. (2014) Lipocalin-type prostaglandin D synthase scavenges biliverdin in the cerebrospinal fluid of patients with aneurysmal subarachnoid hemorrhage. *J. Cereb. Blood Flow Metab.* **34**, 1558–1567 https://doi.org/10.1038/jcbfm.2014.127

73 Millucci, L., Raggiaschi, R., Franceschini, D., Terstappen, G. and Santucci, A. (2009) Rapid aggregation and assembly in aqueous solution of Aβ (25–35).pdf. *J. Biosci.* **34**, 293–303 https://doi.org/10.1007/s12038-009-0033-3

74 Atamna, H. (2006) Heme binding to amyloid-beta peptide: mechanistic role in Alzheimer's disease. *J. Alzheimers Dis.* **10**, 255–266 https://doi.org/10.3233/JAD-2006-102-310

75 Howlett, D., Cutler, P., Heales, S. and Camilleri, P. (1997) Hemin and related porphyrins inhibit beta-amyloid aggregation. *FEBS Lett.* **417**, 249–251 https://doi.org/10.1016/S0014-5793(97)01290-8

76 Linse, S. (2017) Monomer-dependent secondary nucleation in amyloid formation. *Biophys Rev.* **9**, 329–338 https://doi.org/10.1007/s12551-017-0289-z

77 Rutardottir, S., Karnaukhova, E., Nantasenamat, C., Songtawee, N., Prachayasittikul, V., Rajabi, M. et al. (2016) Structural and biochemical characterization of two heme binding sites on alpha1-microglobulin using site directed mutagenesis and molecular simulation. *Biochim. Biophys. Acta* **1864**, 29–41 https://doi.org/10.1016/j.bbapap.2015.10.002

78 Grishkovskaya, I., Paumann-Page, M., Tscheliessnig, R., Stampler, J., Hofbauer, S., Soudi, M. et al. (2017) Structure of human promyeloperoxidase (proMPO) and the role of the propeptide in processing and maturation. *J. Biol. Chem.* **292**, 8244–8261 https://doi.org/10.1074/jbc.M117.775031

79 Thompson, E.J. (1995) Cerebrospinal fluid. *J. Neurol. Neurosurg. Psychiatry* **59**, 349–357 https://doi.org/10.1136/jnnp.59.4.349

80 Mase, M., Yamada, K., Iwata, A., Matsumoto, T., Seiki, K., Oda, H. et al. (1999) Acute and transient increase of lipocalin-type prostaglandin D synthase (beta-trace) level in cerebrospinal fluid of patients with aneurysmal subarachnoid hemorrhage. *Neurosci. Lett.* **270**, 188–190 https://doi.org/10.1016/S0304-3940(99)00494-2

81 Schallner, N., Pandit, R., LeBlanc, III, R., Thomas, A.J., Ogilvy, C.S., Zuckerbraun, B.S. et al. (2015) Microglia regulate blood clearance in subarachnoid hemorrhage by heme oxygenase-1. *J. Clin. Invest.* **125**, 2609–2625 https://doi.org/10.1172/JCI78443

82 Asano, T. (1999) Oxyhemoglobin as the principal cause of cerebral vasospasm: a holistic view of its actions. *Crit. Rev. Neurosurg.* **9**, 303–318 https://doi.org/10.1007/s003290050147

83 Mori, T., Nagata, K., Town, T., Tan, J., Matsui, T. and Asano, T. (2001) Intracisternal increase of superoxide anion production in a canine subarachnoid hemorrhage model. *Stroke* **32**, 636–642 https://doi.org/10.1161/01.STR.32.3.636

84 Flemmig, J., Zamocky, M. and Alia, A. (2018) Amyloid beta and free heme: bloody new insights into the pathogenesis of Alzheimer's disease. *Neural Regen Res.* **13**, 1170–1174 https://doi.org/10.4103/1673-5374.235021